RESEARCH ARTICLE

Thermoelectric Properties of $Zr_xIn_xZn_{1-x}O_{1-\delta}$ Thin Films

Prasoon Prasannan[1], N.K. Deepak[1], N.K.Sulfikkarali[2], P. Jayaram[3,*]

[1]Department of Physics, Kannur University, Kerala, 670327, India
[2]Department of Physics, Farook College, Calicut, Kerala 673632, India
[3]Materials Science Laboratory, Department of Physics, MES Ponnani College, Ponnani, Malappuram, Kerala, India

*Corresponding author: E-mail: jayarampnair@gmail.com

DOI: 10.5185/amlett.2021.011596

The variation of thermoelectric properties of Zr_2O_3-In_2O_3-ZnO film system is reported here. The films are fabricated in a chemical composition satisfies the relation $Zr_xIn_xZn_{1-x}O_{1-\delta}$, ($0.01 \geq x \geq 0.04$), through spray pyrolysis technique. XRD analysis shows a switching of preferred crystal growth orientation from (002) to (100) and (101) planes as x increases. The quasi spherical surface morphology was improved on the addition of the cations. A maximum Seebeck coefficient of -159 μV/K was obtained for x = 0.01 at 400K. The decrease in the Seebeck coefficient for higher x values is explained with simplified broadband model. At elevated temperature power factor increased considerably up to 2.33 X 10^{-4} $Wm^{-1}K^{-2}$ for x = 0.03 which was attributed to decrease in sheet resistance at high temperature.

Introduction

The energy generation, conversion and regeneration are the crucial steps in the field of energy and technology research paying attention to the suitable materials with high elemental abundance, non-toxicity and conversion efficiencies [**1-3**]. Considering the energy technology aspects, thermoelectric (TE) properties of materials are regarded as most promising because such materials can convert the waste heat into electricity through a unique phenomenon called the Seebeck effect [**3,4**]. Large amount of heat is being wasted in industries, automobiles and oil mines and this energy can be harvested and converted to electrical energy by the help of thermoelectric materials. Till date Bi_2Te_3 and Sb_2Te_3 alloys are commonly regarded as the best thermoelectric materials due to its higher efficiencies when it is used for room temperature applications [**5**]. Alloying of tellurides and selenides of bismuth and antimony such as $Bi_2(Te_{0.8}Se_{0.2})_3$, $(Sb_{0.8}Bi_{0.2})_2Te3$showed excellent *ZT* and higher n-type carrier concentrations, alongside, p-type $(Sb_{0.8}Bi_{0.2})_2Te_3$ compounds are also extensively investigated [**6**]. Group IV tellurides like PbTe, GeTe or SnTe are widely investigated thermoelectric materials [**6-8**]. Like photovoltaics, thermoelectricity can also be associated with green technology and this has the capacity to contribute to the energy requirement of the society [**9-10**]. But even today, organic thermoelectric materials are less studied compared to the photovoltaic materials. However, thermoelectric materials like polypyrrole reported to exhibit excellent thermal conductivity characteristics [**11**]. But this electric conductivity values need to be improved further for TE applications and most of the current research is directed towards this purpose [**12**]. In comparison with organic thermoelectric material, inorganic thermoelectric materials show promising electronic crystal nature, this favors thermal conductivity from the free carrier acquirable from the lattice [**13**]. Inorganic thermoelectric materials show poor phonon glass character and this can be overcome by introduction of defects in the crystal or by deterioration of crystal quality, doping in crystals is a smart way to implement this. The metal oxides hence become a favorable choice considering the easiness in induced lattice defects [**14**]. The oxides of metal and its combinations are high temperature thermoelectric materials because of its robustness at higher temperatures in which the other metal alloys melts [**15**]. Zinc oxide is a wide band gap material which can offer durability in extreme temperature and chemical environments [**16**]. It has been observed that a reduction in size of materials will reduce the thermal conductivity which in turn will improve the thermoelectric properties of the material. Hence considerable amount of research is focused towards improving the thermoelectric properties of low dimensional materials, especially nano dimensional thin films. Herein, we report the fabrication of $Zr_xIn_xZn_{1-x}O_{1-\delta}$ thin films at changing the concentrations of zirconium and indium in ZnO thin films by spray pyrolysis technique on quartz substrate. The structure and surface morphology of the films are reported here. The thermoelectric Seebeck effect, thermoelectric power factor and sheet resistance are measured and reported in the article.

Materials and methods

A 0.2 molar precursor solution was made by ultrasonically dissolving Zinc acetate dihidrate in a solvent containing methanol, deionised water and acetic acid in the ratio 65:25:10. Separate 0.2 molar solutions of zirconium acetyl

acetonate and indium nitrate were made in the same solvent and were used as respective source for zirconium and indium. $Zr_xIn_xZn_{1-x}O_{1-\delta}$ at different *x* values was prepared by adding zirconium acetyl acetonate and indium nitrate solutions in the parent solution in calculated amount, by limiting total volume to 25ml. The solutions were then sprayed on to triple stage cleaned $1cm^2$ fused silica substrate using Holmarc HO-TH 04 automated spray pyrolysis system. The substrate temperature was kept at 400^0C at a flow rate of 3ml/minute and then samples were subjected to vacuum annealing (10^{-5}m-bar) at 400^0C for two hours. The crystal structure of the samples was analyzed with X-ray diffraction technique using Rigaku Miniflex diffractometer with X-rays with a wavelength of 1.54A°. Scanning Electron Micrographs (SEM) images obtained by VEGA-TESCAN attached with Energy Dispersive Spectra (EDS) analyzer with an accelerating voltage of 30 KeV. Hall Effect measurement was performed using Ecopia HMS 3000 Hall measurement system. The Seebeck coefficients were obtained from Ulvac ZEM 3 system at room temperature to 400^0C.

Results and discussion

Structure and surface morphology

The XRD diffractograms were compared with ICDD card 36-1451 [**16**] and the formation of hexagonal wurtzite structured particle were confirmed from the plot exhibited in **Fig. 1**. Changes in the preferential growth orientation from (002) plane to (100) and (101) planes were observed as x component increases from 0.01 to 0.04. The presence of different cations on the substrate surface during film growth might have affected the surface energy. The change in growth orientation with doping concentration can be attributed to this change in surface energy [**16,17**]. Even though the phase purity was sustained by the films, the crystalline quality was found decreasing with increase in x value. A continuous decrease in crystallite size was also observed with increasing level indium and zirconium contents. This variation might be due to the stress developed in the crystal when dopants atoms are incorporated into grain boundaries. The film showed a preferential orientation along (002) plane at $2\theta = 34.64°$ indicating that ZnO tends grow perpendicular to the substrate surface [**17,18**]. Two very weak peaks were observed at $2\theta = 62.86°$ and 72.67^0 corresponding to (103) and (004) planes respectively. The XRD result showed that the crystalline quality of the film deteriorated up on zirconium/Indium content increase. Similar behavior had been reported earlier for Zr doped ZnO thin films by spray pyrolysis method, which attributed the effect to interstitial inclusion of dopant atoms to the ZnO lattice [**19**]. This will lead to formation of the stresses by the difference in ion size between zinc and zirconium. Another reason can be the formation of extrinsic stress by the lattice mismatch between the film and substrate for high x values. The formation of (100) and (101) peaks can be attributed to the contribution of Zr^{4+} ions. Similar behavior has been reported by Ray-Hua Horng *et. al.*, during deposition of Ga doped ZnO thin films by MOCVD method [**20**]. Beyond Zr doping level of 4 at% the (100) and (101) peaks became more intense than (002) peaks i.e., switching of preferred orientation from (002) to (100) direction occurs.

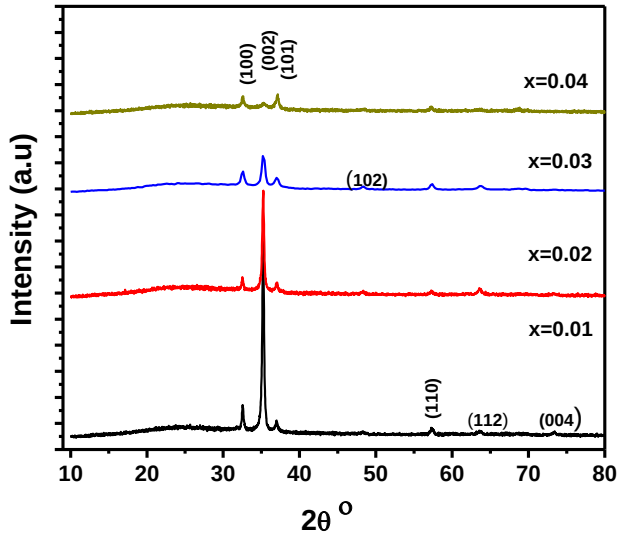

Fig. 1. X-ray diffraction pattern of Zr_xIn_xZnO of thin films showing single phase wurtzite growth of films with preferential orientations tends to change as the x contents increases.

The SEM analysis of the samples revealed a uniform distribution of rice like grains on the substrate, each and every sample show non porous random distribution of particle on the surface. At higher order doping, surface morphology changed to quasi-spherical particle configuration. The particle size was not uniform but showed variation from 200 to 700 nm. The amount of elements on the film surface estimated from energy dispersive spectra (not shown in this report).

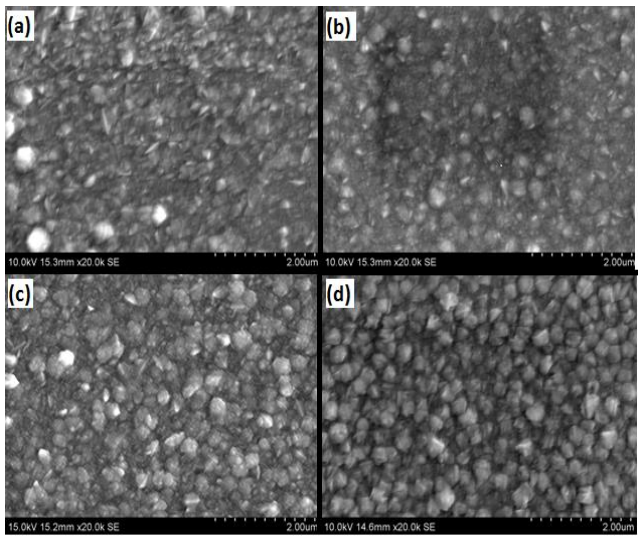

Fig. 2. Scanning Electron Micrographs showing uniform growth of grains like particle on the substrate (a) x = 0.01 (b) x = 0.02 (c) x = 0.03 (d) x = 0.04.

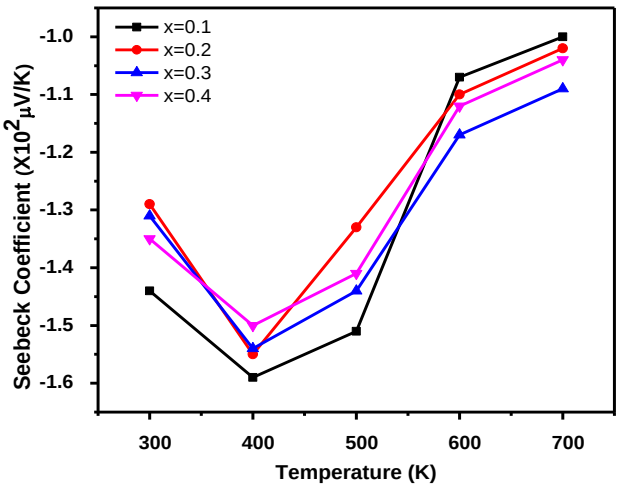

Fig. 3. The variation of Seebec Coefficient with respect to the temperature for different x values in $Zr_xIn_xZn_{1-x}O_{1-\delta}$

DC electrical properties and thermoelectric properties

The Seebeck coefficients of the films were measured from room temperature to 700K. All samples exhibited negative value for Seebeck coefficient indicating the *n* type semiconducting nature of the films. The variation of Seebeck coefficient with temperature for various concentrations of films is shown in **Fig. 3**. Highest value for Seebeck coefficient was exhibited by samples at x = 0.01 at measuring temperatures. As the concentration increases the Seebeck coefficient values tends to decrease. The introduction of dopant atoms in the ZnO matrix will directly induce considerable increase in the concentration of free carriers in conduction band. The excess concentration of carriers will modify the Fermi level of the semiconductors and this in turn directly affects the Seebeck coefficient of the film [**20**]. According to simplified broadband model, the dependence of Seebeck coefficient on carrier concentration is given by the relation [**21**].

$$S = -\left(\frac{k_B}{e}\right)\ln\left(\frac{N_v}{n_e}\right) + A$$

Where k_b is the Boltzmann constant, N_e is the density of states, n_e I the carrier concentration and A is transport constant.

Based on this relation the reduction in Seebeck coefficient with doping is attributed to the increase in carrier concentration on doping. All samples show maximum value for Seebeck coefficient at 400K and then reduce gradually with temperature. Among doped samples the maximum value for Seebeck coefficient of 159 μV/K was shown by sample with x = 0.01 at 400K. This value reduces to 100 μV/K at 700K. At higher temperature range sample with x = 0.03 shows maximum Seebeck coefficient value of 110 μV/K. This value is very promising when compared to other ZnO based thermoelectric materials. The energy dependence on carrier density influences the Seebeck coefficient and this is considerable when the dimension of the materials is too low (in the range of 20A0). In this study, the dimension of films are higher and the probability the effect of energy dependence is neglected. On the other hand, the energy dependence of mobility affects the Seebeck coefficient of the material and this is more dominant in higher dimensional materials than the carrier density. The grain boundary scattering determines the carrier mobility largely since the carrier may scatter at inhomogeneous grain boundaries thus causes reduction in it [**21**]. Thus, the grain size plays important role in determining the Seebeck coefficient of a 2D material [**22**].

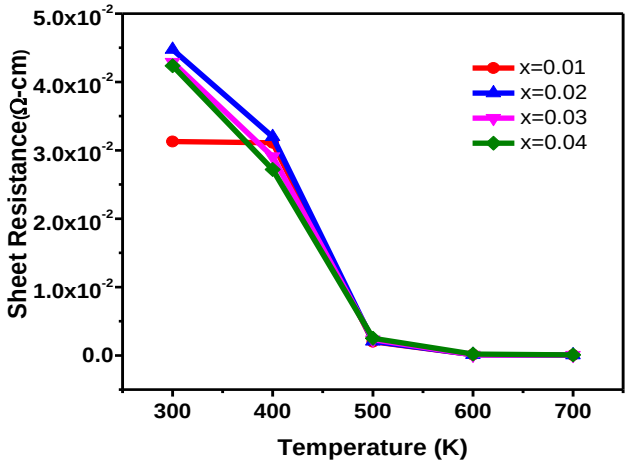

Fig. 4. The sheet resistance of the samples, indicating decrease in in sheet resistance as increase in x contents.

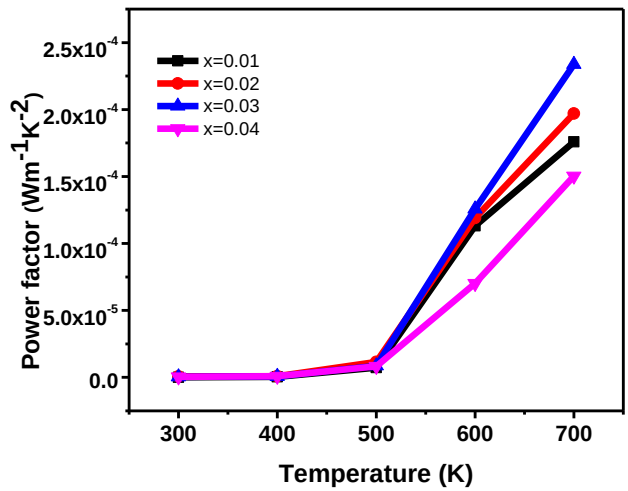

Fig. 5. The power factor of the films plotted against the variations in temperature and measured for samples with different compositions.

The power factor (PF) variation with doping concentration at different temperature is plotted in **Fig. 5**. Samples show moderate power factors up to the temperature 500K. However, at high temperature power factor increases considerably. The x = 0.03 sample shows maximum power factor of 2.33 X 10^{-4} $Wm^{-1}K^{-2}$.PF was observed to decrease for samples with higher level of doping. The resistivity of the films at different

temperatures is shown in **Fig. 4**, the resistivity showed a steep drop in value at high temperatures. The carrier electrons gain thermal energy at high temperatures which resulted in the reduction of resistivity. Resistivity of the order 10^{-7} Ohm m was showed by doped samples at 600-700K regions. The power factor depends on the conductivity of the films by the relation [**23**].

$$PF=\alpha^2 \sigma$$

where α is the Seebeck coefficient and σ is the electrical conductivity

Since the power factor is directly proportional to the electrical conductivity, the peaking of power factor at elevated temperature can be explained by the drop in resistivity at high temperatures. Despite a decrease in absolute value of Seebeck coefficient, PF shows an increase with temperature, owing to the dominant decrease in sheet resistance with temperature.

Conclusion

$Zr_xIn_xZn_{1-x}O_{1-\delta}$ thin films were deposited on fused silica substrates using spray pyrolysis technique at a surface temperature 400°C. X-ray diffraction pattern revealed a change in preferred growth orientation for higher order doped samples. This change was attributed to change in surface energy due to the presence of multi cations. Scanning electron micrographs showed non porous surface morphology and dense growth of samples on substrate. The Seebeck coefficient of thin films reduced considerably on increase the x values and this is due to increase in carrier concentration with doping and was in accordance with simplified broad band model. The sheet resistance of each sample is dropped by many orders with increasing temperature. This improvement in conductivity resulted in promising power factors for samples at higher temperatures.

Acknowledgement

The author Jayaram P acknowledge the financial assistance of DST-FIST Level-0 program for setting the laboratory in MES Ponnani College.

Keyword

Zr_2O_3-In_2O_3-ZnO, seebeck effect, thermoelectric materials.

Received: 02 May 2020
Revised: 03 July 2020
Accepted: 17 July 2020

References

1. Kumar, B; Kim, S.W; *Nano Energy*, **2012**, *1*, 342.
2. Su, R.R; Yu,Y.X; Xiao, Y.H; Yang X.F; Zhang, W.D; *International Journal of Hydrogen Energy*,**2018**, *43*, 6040.
3. Eftekhari, E; Broisson, P; Aravindakshan, N; Wu, Z; Cole, I.S; Li,X; Zhao, D; Li, Q; *J. Mater. Chem. A*, **2017**, *5*, 12803.
4. Fan, Z; Du, D; Guan, X; Ouyang, J; *Nano Energy*,**2018**, *51*, 481.
5. Colder, H; Guilmeau, E; Harnois, C; Marinel, S; Retoux, R; Savary, E; *Journal of the European Ceramic Society*, **2011**, *31*, 2957.
6. Li, J; Chen, Z; Zhang, X; Sun, Y; Yang, J; Pei, Y; *NPG Asia Materials*, **2017**, *9*, 353.
7. Li, W; Zheng, L; Ge, B; Lin, S; Zhang, X; Chen, Z; Chang, Y; Pei, Y.; *Advanced Materials*, **2017**, *29*, 1605887.
8. Brinzari, V.; Damaskin, I.; Trakhtenberg, L.; Cho, B.K.; Korotcenkov, G.; et. al., *Thin Solid Films*, **2014**, *552*, 225.
9. Russ, B.; Glaudell, A.; Urban, J.J.; Chabinyc, M.L.; Segalman, R.A.; *Nature Reviews Materials*, **2016**, *1*, 16050.
10. Yao, C.J.; Zhang, H.L.; Zhang, Q.; *Polymers*, **2019**, *11*, 107.
11. Jian, Xie; et al., *Chem. Asian J.*, **2016**, *11*, 1489.
12. Wu, J.; Sun, Y.; Pei, W.B.; Huang, L.; Xu, W.; Zhang, Q.; *Syn. Met.*, **2014**, *196*, 173.
13. Zhao, W.; Zhang, F.; Dai, X.; Jin, W.; Xiang, L.; *Adv Mater.*, **2019**, *131*, 19170.
14. Saini, S.; Mele, P.; Honda, H.; Suzuki, T.; Matsumoto, K.; *Thin Solid Films*,**2016**, *605*, 289.
15. Liu, W.; Hu, J.; Zhang, S.; Deng, M.; Han, C.G.; Liu, Y.; *Materials Today Physics*, **2017**, *1*, 50.
16. Lupan, O.; Pauporte, T.; Chow, L.; Viana, B.; Pelle, F.; *Applied Surface Science*, **2010**, *256*, 1895.
17. Shabannia, R.; *Progress in Natural Science: Materials International*, **2015**, *25*, 95.
18. Gokulakrishnan, V.; Parthiban, S.; Jeganathan, K.; Ramamurthy, K.; *Applied Surface Science*, **2011**, *257*, 9068.
19. Horng, R.H.; Ou, S.L.; Huang, C.Y.; Ravadgar, P.; Wu, C.I.; *Thin Solid Films*, **2016**, *605*, 30.
20. Colder, H.; Guilmeau, E.; Harnois, C.; Marinel, S.; Retoux, R.; Savary, E.; *Journal of the European Ceramic Society*, **2011**, *31*, 2957
21. Mao, J.; Liu, Z.; Ren, Z.; *NPJ Quantum Materials*, **2016**,*1*, 16028.
22. Gao, Y.W.; He, Y.Z.; Zhu, L.L.; *Chinese Science Bulletin*, **2010**, *55*, 16.
23. Fan, P.; Li, Y.; Zheng, Z.; Lin, Q.; Luo, J.; Liang, G.; *Applied Surface Science*, **2013**, *284*, 145.